Discretization Error Analysis in the Contrast Source Inversion Algorithm

Discretization Error Analysis in the Contrast Source Inversion Algorithm

Valeria Mariano, Jorge A. Tobon Vasquez, Francesca Vipiana
Dept. of Electronics and Telecommunications, Politecnico di Torino, Torino, Italy,
email:{valeria_mariano, jorge.tobon, francesca.vipiana}@polito.it

***Abstract*—This paper describes the use of the contrast source inversion method combined with the finite element method for the numerical solution of 3-D microwave inversion problems. In particular, this work is focused on the discretization of the involved physical vector quantities, analyzing the impact of the chosen discretization on the solution process with the goal of optimizing the implemented algorithm in terms of accuracy, memory requirements and computational cost.**

***Index Terms*—microwave imaging, finite element method, contrast source.**

I. Introduction

The contrast source inversion (CSI) method is widely used in the numerical solution of microwave inversion problems. It belongs to family of non-linear iterative algorithms, and, despite to a possible high computational cost, it allows accurate quantitative reconstructions. The CSI method has different applications' fields, that have in common the goal to determine location, shape and constitutive properties of a specific target. For instance, it is used to reconstruct the distribution of earth electrical conductivity in cross-well imaging [1], in food industry for detecting spoilage in grain bins using microwave imaging [2], in medical applications such as dosimetry, oncology [3] and brain stroke imaging [4].

One of the first CSI formulation for 2-D problems using integral equations (IE) is described in [5], where a multiplicative regularization is proposed and the results obtained with several 2-D numerical examples are used to discuss the performance of the formulation. However, in some particular case, for example when the background is in-homogeneous or the Green's function is not available in a closed form, the IE formulation is not efficient. In order to overcome this limitation of CSI-IE, a finite difference (FD) formulation of CSI method is presented in [6]. However, also the CSI-FD method is limited, because it has difficulties in modelling boundaries of arbitrary shape. A CSI formulation that exploits the finite element method (FEM) to discretize the domain is described in [4], where the algorithm is applied to 2-D transverse magnetic (TM) problems.

Here, the CSI algorithm is combined with an in-house 3-D FEM solver [7] with the final aim to apply it for brain stroke imaging, thanks to the known dielectric contrast at microwave frequencies between healthy brain tissues and the stroke area [8]–[10]. In particular, this paper proposes different discretizations of the involved physical vector quantities in the considered 3-D domain, analyzing the impact on the solution process in terms of accuracy, memory requirements and computational cost.

The paper is organized as follow. Section II contains a brief description of the CSI algorithm, while Sect. III is focused on the proposed discretizations of the physical quantities. Then, the impact of the different dicretizations in the solution process is analyzed in Sect. IV and the conclusions are summarized in Sect. V.

II. The Contrast Source Inversion Method

In this section, a brief description of the contrast source inversion method in a 3-D scattering problem is given.

The considered scenario is shown in Fig. 1. The whole 3-D domain is indicated with Ω and it is filled with a background medium with known complex relative permittivity, ϵ_b. The region of interest, D, is inside Ω and contains the target with unknown complex relative permittivity, ϵ_r. The T antenna probes are located on the surface S at the boundary of D.

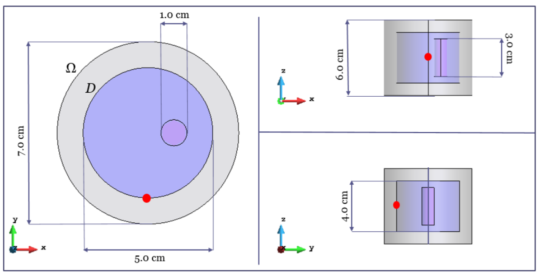

Fig. 1. Geometry of the model. The whole domain is Ω, the domain of interest is D. The background relative dielectric constant is $\epsilon_b = 22.70 - j6.13$, instead the dielectric constant in the target is $\epsilon_r = 63.06 - j26.48$. The red spot identifies the position of one of the probe.

When the t-th antenna probe illuminates Ω without the target, the corresponding radiated electric field is called incident field, $\underline{E}_t^{\mathrm{inc}}(\underline{r})$, while, if the target is present, it is called total field, $\underline{E}_t^{\mathrm{tot}}(\underline{r})$. Then, the scattered field, $\underline{E}_t^{\mathrm{sct}}(\underline{r})$, is equal to $\underline{E}_t^{\mathrm{tot}}(\underline{r})$ minus $\underline{E}_t^{\mathrm{inc}}(\underline{r})$. The dielectric contrast, $\chi(\underline{r})$, between the background medium and the target, is defined as

$$\chi(\underline{r}) \triangleq \frac{\epsilon_r(\underline{r}) - \epsilon_b(\underline{r})}{\epsilon_b(\underline{r})}. \tag{1}$$

Moreover, an additional quantity, called contrast source (also called secondary, induced or passive source [11, Ch. 5]), is defined as

$$\underline{\omega}_t(\underline{r}) \triangleq \chi(\underline{r})\, \underline{E}_t^{\mathrm{tot}}(\underline{r}), \tag{2}$$

and it links the total field radiated by the t-th antenna and the dielectric contrast for each considered point $\underline{r}$. Equation (2) is also known as object equation. For each antenna t, $\underline{E}_t^{\rm sct}$ and $\underline{\omega}_t$ are related together via the wave equation [12]:

$$\nabla \times \nabla \times \underline{E}_t^{\rm sct}(\underline{r}\ ) - k_b^2\,(\underline{r})\underline{E}_t^{\rm sct}(\underline{r}\ )\ = k_b^2(\underline{r})\,\underline{\omega}_t(\underline{r}), \quad (3)$$

where $k_b^2(\underline{r}) = \omega^2 \mu_0 \epsilon_0 \epsilon_b(\underline{r})$ is the background medium wave number, ω is the angular frequency, and μ_0 and ϵ_0 are the free space permeability and permittivity, respectively.

The solution of the non-linear inverse problem is obtained through the minimization of a cost functional that measures the mismatch between known (measured) data and the corresponding ones, predicted by the numerical model. The CSI cost functional can be expressed as

$$F^{\rm CSI}(\chi_n, \underline{\omega}_{t,n}) = F^S(\underline{\omega}_{t,n}) + F^D(\chi_n, \underline{\omega}_{t,n}), \quad (4)$$

where F^S measures the mismatch at the antenna locations on S , while F^D is the mismatch in the region of interest D. The minimization of $F^{\rm CSI}$ is performed through an iterative optimization that, at each iteration n, updates alternatively $\underline{\omega}_{t,n}(\underline{r})$ (for $t = 1, \ldots, T$), and $\chi_n(\underline{r})$ [4].

III. Discretization of the CSI Variables

In order to numerically implement the described CSI algorithm, the whole considered 3-D domain Ω as well as its associated vector and scalar variables have to be properly discretized. In the following, two different discretization approaches are described and, then, numerically validated in Sect. IV.

The volume Ω is discretized via tetrahedra cells. The complex relative permittivity is evaluated at each cell barycenter and considered constant within the cell. The dielectric contrast can be approximated as

$$\chi(\underline{r}) \cong \sum_{i=1}^{I} \chi_i p_i(\underline{r}), \quad (5)$$

where I is the total number of tetrahedra in Ω, each coefficient χ_i is the dielectric contrast in the barycenter of the i-th tetrahedron C_i, and

$$p_i(\underline{r}) = \begin{cases} 1 & \underline{r} \in C_i \\ 0 & \text{elsewhere.} \end{cases} \quad (6)$$

For each antenna t, the scattered field $\underline{E}_t^{\rm sct}$ as well as the total one $\underline{E}_t^{\rm tot}$ can be approximated as a linear combination of vector basis functions, $\underline{N}_i(\underline{r})$, as

$$\underline{E}_t^{\rm sct}(\underline{r}) \cong \sum_{i=1}^{E} E_{t,i}^{\rm sct} \underline{N}_i(\underline{r}) \quad (7)$$

$$\underline{E}_t^{\rm tot}(\underline{r}) \cong \sum_{i=1}^{E} E_{t,i}^{\rm tot} \underline{N}_i(\underline{r}) \quad (8)$$

where E is the total number of edges in Ω, and $E_{t,i}^{\rm sct}$ and $E_{t,i}^{\rm tot}$ are the coefficients. Each basis function $\underline{N}_i(\underline{r})$ is associated to the i-th edge of the mesh and defined on the group of tetrahedra that has the i-th edge in common. The selected basis functions are the well-known vectorial and curl-conforming basis functions usually implemented in FEM 3-D problems with tetrahedral discretization. Each $\underline{N}_i(\underline{r})$ has constant tangential component along the i-th edge to which it is associated and no tangential component along the remaining five edges of the tetrahedra where the basis function is defined [13].

A. Standard Discretization

In the standard discretizaton of CSI method [12], for each antenna t, the corresponding contrast source $\underline{\omega}_t$ is discretized as

$$\underline{\omega}_t(\underline{r}) \cong \sum_{i=1}^{I} \underline{\omega}_{t,i}\, p_i(\underline{r}), \quad (9)$$

where $\underline{\omega}_{t,i}$ are *vector* coefficients. Each coefficient corresponds to

$$\underline{\omega}_{t,i} = \chi(\underline{r}_i)\, \underline{E}_t^{\rm tot}(\underline{r}_i), \quad (10)$$

where $\underline{r}_i$ is the barycenter of each tetrehadron for $i = 1, \ldots, I$.

Inserting (7) and (9) into (3) and applying the Galerkin weighted residual testing, we obtain the linear system

$$([U] - [V])\,[E_t^{\rm sct}] = [\underline{R}] \cdot [\underline{\omega}_t], \quad (11)$$

where $[U]$ and $[V]$ are the usual FEM stiffness and mass matrices with dimension $E \times E$. Each element of $[U]$ is

$$[U]_{i,j} = \int_\Omega (\nabla \times \underline{N}_i\ ) \cdot (\nabla \times \underline{N}_j)\, d^3\underline{r}, \quad (12)$$

and each element of $[V]$ corresponds to

$$[V]_{i,j} = \int_\Omega k_b^2\, \underline{N}_i \cdot \underline{N}_j\, d^3\underline{r}. \quad (13)$$

Thanks to chosen test and basis functions, (12) and (13) are known in closed form [13]. $[E_t^{sct}]$ is an array with length E collecting the scattered field coefficients for the transmitter t (7), while $[\underline{R}]$ is a $E \times I$ matrix that collects the *vector* quantities

$$[\underline{R}]_{i,j} = \int_\Omega k_b^2\, \underline{N}_i(\underline{r})\, p_j(\underline{r})\, d^3\underline{r}. \quad (14)$$

Finally, $[\underline{\omega}_t]$ is an array with length I collecting the *vector* contrast source coefficients for the transmitter t (11), and "$\cdot$" denotes the dot product between the elements on the $[\underline{R}]$ rows and $[\underline{\omega}_t]$, respectively.

Using this discretization in the CSI algorithm, the contrast sources coefficients are vectors with three components to be updated at each iteration, and the corresponding discretized opertors are *dyadic*, making the numerical implementation complex. Moreover, during the variables updating at each iteration of the CSI algorithm, the same operations have to be repeated three times to update the three components of the contrast source coefficients with an evident additional computational burden.

B. Alternative Discretization

In order to simplify and speed up the CSI implementation, we propose an alternative discretization for the contrast source variable.

Considering that each basis function $\underline{N}_j$, used to discretize the total radiated field in (8), is defined on a group of K tetrahedra, $C_{j,k}$, with the j-th edge in common, we can write

$$\underline{N}_j(\underline{r}) = \begin{cases} \widetilde{\underline{N}}_{j,k}(\underline{r}) & \underline{r} \in C_{j,k} \\ 0 & \text{elsewhere} \end{cases} \tag{15}$$

with $j = 1, \dots, E$ and $k = 1, \dots, K$. Then, observing that each tetrahedron has six edges, we can associate the discretized total field to each tetrahedron instead to each edge as

$$\underline{E}_t^{\text{tot}}(\underline{r}) \cong \sum_{i=1}^{I} \sum_{e=1}^{6} E_{t,(i,e)}^{\text{tot}} \, \widetilde{\underline{N}}_{i,e}(\underline{r}). \tag{16}$$

Now substituting (16) and (5) into (2), we obtain

$$\begin{aligned} \underline{\omega}_t(\underline{r}) &\cong \left[\sum_{i=1}^{I} \chi_i p_i(\underline{r}) \right] \left[\sum_{e=1}^{6} E_{t,(i,e)}^{\text{tot}} \, \widetilde{\underline{N}}_{i,e}(\underline{r}) \right] \\ &= \sum_{i=1}^{I} \sum_{e=1}^{6} \left(\chi_i \, E_{t,(i,e)}^{\text{tot}} \right) \widetilde{\underline{N}}_{i,e}(\underline{r}) \\ &= \sum_{i=1}^{I} \sum_{e=1}^{6} \omega_{t,(i,e)} \, \widetilde{\underline{N}}_{i,e}(\underline{r}). \end{aligned} \tag{17}$$

where the pulse functions $p_i(\underline{r})$ are omitted because $\widetilde{\underline{N}}_{i,e}(\underline{r})$ are already defined within each cell. Comparing (17) with (9), we can noticed that, with the proposed discretization, the constrast source coefficients are scalars instead of vectors, and their vectorial part is totally contained in the vector basis functions as done in the field discretization with the same kind of basis functions.

Now, the right hand side of (11) is rewritten as

$$([U] - [V]) \, [E_t^{\text{sct}}] = [R][\omega_t]. \tag{18}$$

where the elements of $[R]$ and $[\omega_t]$ are scalars. In particular, $[\omega_t]$ is an array with length $6I$ that collects the contrast course scalar coefficients in (17) and $[R]$ is a $E \times 6I$ matrix with each element equal to

$$[R]_{m,n} = \int_{\Omega} k_b^2 \, \underline{N}_m(\underline{r}) \cdot \widetilde{\underline{N}}_n(\underline{r}) \, d^3\underline{r}, \tag{19}$$

where n is equivalent to the double indexing (i, e) exploited in (17).

This alternative discretization, in which all the coefficients within the discretized wave equation are scalars, simplifies the CSI algorithm implementation and, as shown in the next section, increases the discretization accuracy.

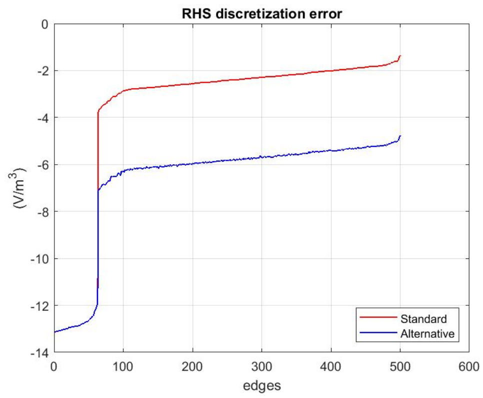

Fig. 2. Difference between the LHS and RHS in (11) and (18)

IV. Numerical Analysis

In this section, the two discretization approaches are numerically analyzed.

The considered 3-D geometry is reported in Fig. 1. The whole domain is Ω and it is filled with a background medium with a complex relative permittivity of $\epsilon_b = 22.70 - j6.13$; the target is a 1 cm cylinder, within the imaging domain D and with relative permittivity $\epsilon_r = 63.06 - j26.48$. The chosen permittivities represent the average brain tissues and the blood at the frequency of 1.1 GHz [10]. The volume Ω is discretized with tetrahedral elements with dimension 5 mm that corresponds to $\lambda/12$ in the background medium. The total and incident fields, radiated within Ω by one probe antenna (located on the surface S at the boundary of D, as shown Fig. 1), are evaluated via an in-house 3-D FEM solver applying absorbing boundary condition at Ω borders.

In Fig. 2, the numerically evaluated right hand side (RHS) of (11) and (18) are compared to the corresponding left hand side (LHS). In particular, the graph shows the element-element difference between the left and right hand sides for the two analyzed discretizations of the contrast source variable. To help the graph readability, the results are sorted and in logarithmic scale, and only the elements where the dielectric contrast is different from zero are shown. We can notice that using the standard discretization the error is around four orders of magnitude higher with respect to using the proposed one. Then, to have quantitative indicators, the L2-norm (η) and the relative L2-norm (η_r) of the difference between the evaluated right and left hand sides are reported in Table I for both discretizations.

TABLE I
Error between RHS and LHS

	η	η_r
Standard	0.19	0.52
Alternative	$7.42 \cdot 10^{-5}$	$2.04 \cdot 10^{-4}$

For a further analysis, we compare the scattered field evaluated solving (11) and (18) with respect the scattered field obtained as difference between the total and incident fields, evaluated with the 3-D FEM solver. Table II shows η and η_r for these quantities. In both Table I and II, the errors values for the proposed discretization are much smaller than the error for the standard one. In the standard discretization, the field in (10) is assumed constant inside each tetrahedron, instead in the alternative discretization the field variation is described with the basis functions. This difference could explain the different behaviour of the error in Table I.

TABLE II
$[E^{\mathrm{sct}}]$ ERROR

	η	η_r
Standard	387.01	0.52
Alternative	0.15	$2.04 \cdot 10^{-4}$

Finally, in order to have an overall vision of discretizations efficiency related to CSI algorithm, the numerical analyses proceeds with the calculation of cost functional (4), considering the exact values of dielectric contrast and contrast sources for the two discretizations (i.e., the cost functional should be ideally zero). As reported in Table III, using the alternative discretization the cost functional is much lower with respect to applying the standard discretization.

TABLE III
COST FUNCTIONAL

	F^S	F^D
Standard	0.27	0.03
Alternative	$4.17 \cdot 10^{-8}$	$4.62 \cdot 10^{-9}$

V. CONCLUSION AND PERSPECTIVES

In this paper, a novel discretization of the contrast source variable is proposed and compared to the standard one. The proposed discretization involve scalar coefficients only, simplifying the CSI implementation. Moreover, a lower discretization error has been verified.

Future work deals with the use of this discretization in the implementaion of the 3-D CSI algorithm with a more realistic scenario and with experimental data obtained with the system described in [9].

ACKNOWLEDGMENT

This work was supported by the Italian Ministry of University and Research under the PRIN project MiBraScan - Microwave Brain Scanner for Cerebrovascular Diseases Monitoring

REFERENCES

[1] A. Abubakar and P. M. van den Berg, "Three-dimensional inverse scattering applied to cross-well induction sensors," *IEEE Transactions on Geoscience and Remote Sensing*, vol. 38, no. 4, pp. 1669–1681, 2000.

[2] A. Zakaria, I. Jeffrey, and J. LoVetri, "Full-vectorial parallel finite-element contrast source inversion method," *Progress in Electromagnetics Research-pier*, vol. 142, pp. 463–483, 2013.

[3] A. Arduino, L. Zilberti, M. Chiampi, and O. Bottauscio, "Csi-ept in presence of rf-shield for mr-coils," *IEEE Transactions on Medical Imaging*, vol. 36, no. 7, pp. 1396–1404, 2017.

[4] A. Zakaria, C. Gilmore, and J. LoVetri, "Finite-element contrast source inversion method for microwave imaging," *Inverse Problems*, vol. 26, pp. 115010–21, 11 2010.

[5] P. M. V. D. Berg and A. Abubakar, "Contrast source inversion method: State of art," in *Progress In Electromagnetics Research*, vol. 34, pp. 189–218, 2001.

[6] A. Abubakar, W. Hu, P. Berg, and T. Habashy, "A finite-difference contrast source inversion method," *Inverse Problems*, vol. 24, p. 065004, 09 2008.

[7] E. A. Attardo, A. Borsic, G. Vecchi, and P. M. Meaney, "Whole-system electromagnetic modeling for microwave tomography," *IEEE Antennas Wirel. Propag. Lett.*, vol. 11, pp. 1618–1621, 2012.

[8] R. Scapaticci, J. Tobon, G. Bellizzi, F. Vipiana, and L. Crocco, "Design and numerical characterization of a low-complexity microwave device for brain stroke monitoring," *IEEE Transactions on Antennas and Propagation*, vol. 66, no. 12, pp. 7328–7338, 2018.

[9] J. A. Tobon Vasquez, R. Scapaticci, G. Turvani, G. Bellizzi, D. O. Rodriguez-Duarte, N. Joachimowicz, B. Duchene, E. Tedeschi, M. R. Casu, L. Crocco, and F. Vipiana, "A prototype microwave system for 3D brain stroke imaging," *SENSORS*, vol. 20, May 2020.

[10] J. A. Tobon Vasquez, R. Scapaticci, G. Turvani, G. Bellizzi, N. Joachimowicz, B. Duchêne, E. Tedeschi, M. R. Casu, L. Crocco, and F. Vipiana, "Design and experimental assessment of a 2D microwave imaging system for brain stroke monitoring," *Int. J. Antennas Propag.*, no. Article ID 8065036, p. 12 pages, 2019.

[11] X. Chen, *Computational methods for Electromagnetic Inverse Scattering*. Wiley-IEEE Press, 1st ed., 2018.

[12] A. Zakaria, *The finite-element contrast source inversion method for microwave imaging applications*. PhD thesis, Univ. of Manitoba, 2012.

[13] J. Jin, *The Finite Element Method in Electromagnetics*. Wiley-IEEE Press, 3rd ed., 2014.